ISSN: 2755-0168

Journal of Biotechnology & Bioinformatics Research

SCIENTIFIC Research and Community

Research Article

Open Access

In silico Prediction and Analysis of Autophagy Related Gene-5 Interacting Proteins and their Physicochemical Features

Nisha and Vijay Paramanik*

Cellular and Molecular Neurobiology and Drug Targeting Laboratory, Department of Zoology, Indira Gandhi National Tribal University, Amarkantak

ABSTRACT

Autophagy related gene-5 (ATG5) acts as a marker for autophagosome formation and initiation of autophagy flux. For performing these functions, ATG5 may interacts with several proteins. Hence, this study aims to identify ATG5 interacting proteins and their regulatory features using *in silico* approaches. Briefly, Search Tool for the retrieval of interacting genes/proteins (STRING) database predicted thirty-four ATG5 interacting proteins. Physicochemical characterization of ATG5 interacting proteins were predicted using expert protein analysis system (ExPASY) Protparam. Out of thirty-four proteins, five were stable with acidic PI and hydrophilic in nature. The secondary structure and amino acid (aa) content were predicted by Self-Optimized Prediction Method from Alignment (SOPMA). ATG5 interacting proteins comprised with α-helix and random coils. In addition, ATG5 interacting proteins were rich in leucine and serine whereas cysteine and histidine were very few. Functional characterization by Secondary Structure Prediction of Membrane Proteins (SOSUI) database predicted five soluble signal peptides and two membrane proteins. Further, motifs of ATG5 interacting proteins were predicted by MOTIF search. Herein, motifs were predicted in prosite pattern, prosite profile and protein family database (pFAM) category. In this study, active sites of ATG5 interacting proteins were predicted by universal protein resource (UniProt) database showing glycyl thioester intermediate sites maximally. In conclusion, predicting different properties and binding sites may contribute a better understanding *of ATG5 regulatory functions and protein-protein interactions that may give potential target for docking studies.*

***Corresponding author**

Vijay Paramanik, Cellular and Molecular Neurobiology and Drug Targeting Laboratory Department of Zoology, Indira Gandhi National Tribal University, Amarkantak (MP)-484887, India.

Received: January 16, 2024; **Accepted:** January 23, 2024; **Published:** February 19, 2024

Keywords: ATG-5, Protein-Protein Interaction, Bioinformatics Tools, Physiochemical Characterization

Abbreviations

ATG3: Autophagy-Related Protein 3
ATG16L1: Autophagy-Related Protein 16-1
ATG12: Autophagy-Related Protein 12
TECPR1: Tectonin Beta-Propeller Repeat-containing Protein 1
ATG10: Autophagy-Related Protein 10
ATG7: Autophagy-Related Protein 7
GABARAP: Gamma-Aminobutyric Acid Receptor-Associated Protein
FADD: FAS-Associated Death Domain
ATG16L2: Autophagy-Related Protein 16-2
GABARAPL1: Gamma-Aminobutyric Acid Receptor-Associated Protein-Like 1
MAP1LC3B: Microtubule-Associated Proteins 1A/1B light Chain 3B
MAP1LC3A: Microtubule-Associated Proteins 1A/1B light Chain 3A
PIK3C3: Phosphatidylinositol 3-Kinase Catalytic Subunit Type 3
BCL2L1: Bcl-2-like 1 (Apoptosis Regulator Bcl-X)
WIPI2: WD Repeat Domain Phosphoinositide-Interacting Protein 2
BECN1: Beclin-1
DDX58: Probable ATP-Dependent RNA Helicase DDX58
IRGM1: Immunity-Related GTPase Family M Protein 1
GABARAPL2: Gamma-Aminobutyric Acid Receptor-Associated Protein-Like 1
RB1CC1: RB1-Inducible Coiled-Coil Protein 1
CASP8: Caspase-8
ATG14: Autophagy-Related Protein 14
PIK3R4: Phosphoinositide 3-Kinase Regulatory Subunit 4
MAVS: Mitochondrial Antiviral-Signaling Protein
SQSTM1: Sequestosome-1
TUFM: Tu Translation Elongation Factor
ATG9A: Autophagy-Related Protein 9
ATG13: Autophagy-Related Protein 13
WDFY3: WD Repeat and FYVE Domain-Containing Protein 3
NBR1: NBR1
UVRAG: UV Radiation Resistance Associated Protein
ATG4B: Autophagy Related 4b
ATG101: Autophagy-Related Protein 101
NOD2: Nucleotide-Binding Oligomerization Domain-containing Protein 2

Introduction

Autophagy is essential to maintain organism's homeostasis by regulating basic metabolic operations inside cells to diseases like neurodegenerative disorders and lysosomal disorders etc. However, aggregated cargoes, dysfunctional organelles, random cytoplasmic proteins and stored nutrients are controlled

by autophagy [1]. Autophagy related gene-5 (ATG5) shows significant role in the development of autophagosome structure that after engulfing degraded proteins fuses with lysosomes to form autophagolysosomal complex for further recycling [2,3].

ATG5 contains 275 amino acids, located on the chromosome 10 in mouse. It acts after conjugating with autophagy-related protein 12 (ATG12) and autophagy-related protein 16l-1 (ATG16l1) forming ATG5-ATG12-ATG16l1 complex. ATG5 shows crucial role in central nervous system (CNS) development and neuronal plasticity showed that crossing conditional ATG5 knockout mice lead to axonal swelling especially in terminal membrane regions [4,5]. Therefore, ATG5 may show role in the regulation of membrane structures near axons. Several computational methods have been used to determine membrane dynamics and predict their functions. In autophagy, the routine clearance of degraded proteins from neuronal cells is an essential step to prevent proteotoxicity.

Protein-protein interaction (PPI) network help us to analyze various molecular function, biological processes and cellular components [6]. In molecular function proteins catalytic activity can be determined. ATG5 induces catalysis by reorienting cysteine-threonine residue of autophagy-related protein 3 (ATG3) conjugate activity. In biological function ATG5 cellular signaling mechanisms and metabolic pathway can be determined. Further, intracellular components show the compartment of the cells where proteins function. These components can be predicted by different methods that predicts signal sequences, membrane association or post- translational modifications. Therefore, various computational tools like MOTIF search, SOSUI, SOPMA etc were used to predict these parameters.

During depression, changes in the energy conversion caused by reduced degradation rate of specific proteins are observed. This may be due to blocking of energy metabolism by mitochondrial autophagy process. In stress conditions, ATG5 maintains mitochondrial membrane potential [7]. A newborn mouse without ATG5 dies within a day due to energy reduction [8]. This shows the efficient relevance of autophagy.

These proofs systemic ablation of core autophagy genes might lead to embryonic or perinatal lethality [9].

Thus, the present study focuses *in silico* prediction of ATG5 interacting proteins as well as their physicochemical, structural and functional characteristics. Predicted structural and molecular function of ATG5 interacting proteins sequence were retrieved using STRING server. ExPASY database was used to predict physicochemical properties namely molecular weight, isoelectric point (pI), extinction coefficient, instability index, protein charges, aliphatic index and grand average of hydropathy (GRAVY), while SOPMA server was used to predict functional properties like secondary structure and MOTIF search and InterPro database was used to identify motifs and active sites respectively. In silico analysis therefore helpful to develop pharmacokinetically safe and stable molecules. Moreover, it may give potential target for docking studies.

Materials and Methods

Enlisting ATG5 Interacting Proteins

The protein sequence for *Mus musculus* ATG5 was retrieved using STRING database(https://string-db.org/) and confirmed from National Centre for Biotechnology Information (NCBI) (Protein ID: NP_444299) STRING database is an in-memory database which is used for cataloging protein sequences and associated information. STRING is a database that keeps track of known or expected protein interactions based on four different sources: genomics, high-throughput studies, conserved co-expression and previously published literature.

Physicochemical Characteristics

Bioinformatics relies largely on physicochemical properties, especially for analysing and predicting biological macromolecules like proteins and nucleic acids. These characteristics arise from the molecular and physical qualities of nucleotide bases (for nucleic acids) or amino acids (for proteins). The physical and chemical attributes, such as molecular weight, theoretical pI, amino acid composition, extinction coefficient, instability index, aliphatic index and grand average of hydropathy (GRAVY) of the ATG5 proteins were computed using ExPASY ProtParam tool (http://web.expasy.org/protparam/).

Secondary Structure Prediction

The secondary structure is very popular feature used to encode structure information of amino acids in PPI site prediction. The secondary structure properties like the α-helix, β-turn, extended strand, random coil and turn of amino acid sequences of ATG5 proteins were predicted using self-optimized prediction method with alignment (SOPMA) in percentage (https://npsa-prabi.ibcp.fr/cgi-bin/npsa_automat.pl?page=/NPSA/npsa_sopma.html).

Functional Characterization

In bioinformatics, functional characterisation of proteins involves identifying and understanding the functions, relationships, and biological activities of proteins. Since proteins are essential to many cellular functions, study biological systems require an understanding of this process. ATG5 interacting proteins functional characterization like transmembrane region and their solubility were predicted using SOSUI server (https://harrier.nagahama-i-bio.ac.jp/sosui/mobile/).

Prediction of Motifs and Families of ATG5 Interacting Proteins

Motif search is a synchronised web resource for identification of protein motifs by PROSITE and families by using pFAM for investigating their interactions (https://www.genome.jp/tools/motif/). The MOTIF search database includes a range of analysis and visualisation tools in addition to manually selected hidden Markov models for many different fields [10].

Prediction of Active Sites of ATG5 Interacting Proteins

A crucial component of structural bioinformatics and bioinformatics in general is the prediction of interacting proteins' active sites. Finding these areas is useful for drug discovery, enzyme engineering, and functional annotation as well as for understanding the molecular mechanisms driving protein-protein interactions. ATG5 interacting proteins active sites were predicted using InterPro database. Prediction of active sites gives more idea for protein-protein interaction studies.

Results

Physicochemical Characterization

A list of thirty-four ATG5 interactive proteins were found as mentioned in Table 1 and Figure. 1, based on the STRING server. These databases provide information on proteins identified in primary protein databases such as PDB, SWISS PROT and others [11].

Table 1: ATG5 Interacting Proteins Retrieved from STRING

S.N	Gene Name	Protein Name	Accession Number	Score
1.	ATG3	Autophagy-related protein 3	NP_080678	0.999
2.	ATG16L1	Autophagy-related protein 16-1	AAH49122	0.999
3.	ATG12	Autophagy-related protein 12	NP_080493	0.999
4.	TECPR1	Tectonin beta-propeller repeat-containing protein 1	NP_081686	0.999
5.	ATG10	Autophagy-related protein 10	XP_006517389	0.998
6.	ATG7	Autophagy-related protein 7	XP_036008260	0.998
7.	GABARAP	Gamma-aminobutyric acid receptor-associated protein	NP_062723	0.996
8.	FADD	FAS-associated death domain	AAA97876	0.996
9.	ATG16L2	Autophagy-related protein 16-2	NP_001104581	0.996
10.	GABARAPL1	Gamma-aminobutyric acid receptor-associated protein-like 1	NP_065615	0.994
11.	MAP1LC3B	Microtubule-associated proteins 1A/1B light chain 3B	NP_080436	0.993
12.	MAP1LC3A	Microtubule-associated proteins 1A/1B light chain 3A	NP_080011	0.992
13.	PIK3C3	Phosphatidylinositol 3-kinase catalytic subunit type 3	NP_852079	0.991
14.	BCL2L1	Bcl-2-like 1 (apoptosis regulator Bcl-X)	XP_0111237562	0.990
15.	WIPI2	WD repeat domain phosphoinositide-interacting protein 2	NP_848485	0.990
16.	BECN1	Beclin-1	AAH05770	0.989
17.	DDX58	Probable ATP-dependent RNA helicase DDX58	EDL05445	0.988
18.	IRGM1	Immunity-related GTPase family M protein 1	SDA08570	0.987
19.	GABARAPL2	Gamma-aminobutyric acid receptor-associated protein-like 1	NP_080969	0.986
20.	RB1CC1	RB1-inducible coiled-coil protein 1	NP_033956	0.985
21.	CASP8	Caspase-8;	CAJ18374	0.978
22.	ATG14	Autophagy-related protein 14	NP_766187	0.971
23.	PIK3R4	Phosphoinositide 3-kinase regulatory subunit 4	NP_001074778	0.971
24.	MAVS	Mitochondrial antiviral-signaling protein	NP_001193314	0.970
25.	SQSTM1	Sequestosome-1	NP_035148	0.967
26.	TUFM	Tu translation elongation factor	NP_766333	0.961
27.	ATG9A	Autophagy-related protein 9	EDL00374.1	0.949
28.	ATG13	Autophagy-related protein 13	NP_663503	0.943
29.	WDFY3	WD repeat and FYVE domain-containing protein 3	NP_766470	0.930
30.	NBR1	NBR1	AAC53025	0.925
31.	UVRAG	UV radiation resistance associated protein	NP_848750	0.913
32.	ATG4B	Autophagy related 4b	NP_777363	0.911
33.	ATG101	Autophagy-related protein 101	XP_006521373	0.910
34.	NOD2	Nucleotide-binding oligomerization domain-containing protein 2	AAN84594.1	0.906

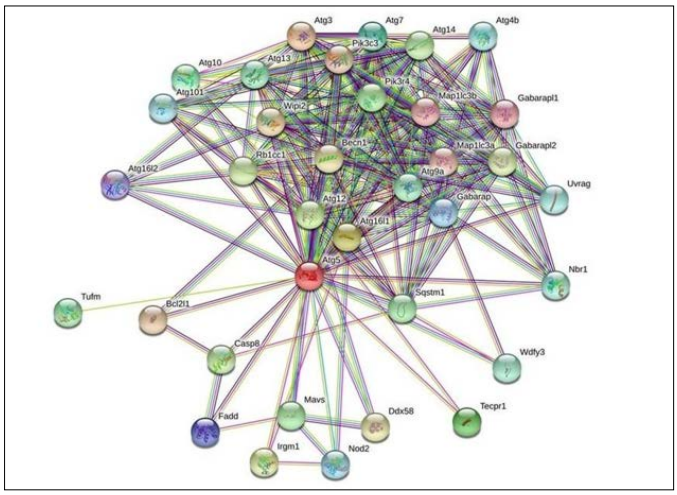

Figure 1: The Figure Indicates STRING Network view for ATG5 Interacting proteins. Coloured Nodes represent Query Proteins and First Shell of Interaction, Filled Nodes Represent some 3D Structure is known and Predicted. Coloured lines between Proteins Indicated Various types of Interactions.

Theoretical pI

Theoretical pI (isoelectric point) of a protein sequence is largely determined by amino acid composition of proteins (Table 2), which is based on a combination of dissociation constant (pKa) values of the constituent amino acids. pI values have often been used in protein isolation, separation, purification, crystallization and other operations to distinguish between proteins and to create various buffer systems [12,13]. Here twenty-four ATG5 interacting proteins namely: ATG3, ATG16l1, autophagy-related protein 12 (ATG12), tectonin beta-propeller repeat-containing protein 1 (TECPR1), autophagy-related protein 10 (ATG10), autophagy-related protein 7 (ATG7), FAS-associated death domain (FADD), autophagy-related protein 101 (ATG101), autophagy-related protein 13 (ATG13), autophagy-related protein 4B (ATG4B), autophagy-related protein 9A (ATG9A), Bcl-2-like 1 (apoptosis regulator Bcl-X) (BCL2L1), Beclin-1 (BECN1), Caspase-8 (CASP8), Probable ATP-dependent RNA helicase DDX58 (DDX58), mitochondrial antiviral-signaling protein (MAVS), (NBR1), phosphatidylinositol 3-kinase catalytic subunit type 3 (PIK3C3), phosphatidylinositol 3-kinase catalytic subunit type 4 (PIK3R4), RB1-inducible coiled-coil protein 1 (RB1CC1), Sequestosome-1 (SQSTM1), WD repeat and FYVE domain-containing protein 3 (WDFY3), WD repeat domain phosphoinositide-interacting protein 2 (WIPI2) and nucleotide-binding oligomerization domain-containing protein 2 (NOD2) showed value lower than 7 indicating their acidic nature and other ten proteins i.e., Gamma-aminobutyric acid receptor-associated protein (GABARAP), autophagy-related protein 16l-2 (ATG16L2), gamma-aminobutyric acid receptor-associated protein-Like 1 (GABARAPL1), gamma- aminobutyric acid receptor-associated protein-Like 2 (GABARAPL2), autophagy-related protein 14 (ATG14), immunity-related GTPase family M protein 1 (IRGM1), microtubule- associated proteins 1A/1B light chain 3A (MAP1LC3A), microtubule-associated proteins 1A/1B light chain 3B (MAP1LC3B), Tu translation elongation factor (TUFM), and UV radiation resistance associated protein (UVRAG) had pI value greater than 7 showing basic nature (Table 2).

Table 2: Computed Physicochemical Properties of ATG5 Interacting Proteins

S.N	Protein	No. of AA	M.W(Da)	pI	-R	+R	Extinction Coefficient	Instability Index	Aliphatic Index	GRAVY
1.	ATG3	314	35796.30	4.63	62	30	46340-45840	41.84 Unstable	78.85	-0.498
2.	ATG16l1	623	69830.66	5.97	93	82	72920-72420	54.73 Unstable	84.56	-0.512
3.	ATG12	141	15207.37	4.90	19	14	15595-15470	59.29 Unstable	82.98	-0.240
4.	TECPR1	1166	130265.96	6.06	134	119	375880-374130	42.49 Unstable	67.34	-0.496
5.	ATG10	211	24278.56	5.35	27	18	41285-40910	42.72 Unstable	78.06	-0.354
6.	ATG7	698	77520.17	5.97	79	69	84560-83310	37.37 Stable	87.48	-0.102
7.	GABARAP	117	13918.04	8.73	18	20	11920	46.09 Unstable	80.77	-0.534
8.	FADD	205	22960.21	5.77	34	31	12615-12490	47.34 Unstable	97.95	-0.380
9.	ATG16l2	623	69241.20	8.58	75	82	81900-80900	45.98 Unstable	84.25	-0.478
10.	GABARAPL1	117	14044.07	8.67	19	21	14900	37.17 Stable	69.91	-0.794

11.	GABARAPL2	117	13666.84	7.81	17	18	18450-18450	32.98 Stable	84.87	-0.316
12.	ATG101	218	25001.70	5.81	33	29	27180-26930	44.41 Unstable	89.27	-0.284
13.	ATG13	479	52615.44	5.02	64	42	27890-27390	42.32 Unstable	77.12	-0.283
14.	ATG14	492	55388.45	7.93	68	70	57005-56380	52.86 Unstable	72.95	-0.697
15.	ATG4B	393	44403.41	4.93	53	34	66640-65890	45.18 Unstable	81.15	-0.206
16.	ATG9A	847	95222.28	6.44	83	74	120750-119750	54.81 Unstable	90.74	-0.108
17.	BCL2L1	233	26132.02	4.87	32	21	47440	39.11 Stable	73.26	-0.386
18.	BECN1	448	51588.95	4.86	75	52	55390-54890	41.14 Unstable	74.87	-0.648
19.	CASP8	480	55356.88	5.12	84	65	34350-33350	52.60 Unstable	78.60	-0.589
20.	DDX58	926	105975.44	6.23	134	125	95240-93740	40.81 Unstable	86.06	-0.416
21.	IRGM1	409	46551.80	8.56	47	52	41995-41370	50.68 Unstable	92.89	-0.179
22.	MAP1LC3A	121	14272.46	8.73	16	18	5960	63.72 Unstable	82.07	-0.522
23.	MAP1LC3B	125	14616.87	8.01	17	18	5960	65.99 Unstable	88.00	-0.393
24.	MAVS	503	53398.90	5.97	44	39	37400-36900	61.62 Unstable	74.89	-0.335
25.	NBR1	988	109957.62	5.01	148	98	84560-83310	62.34 Unstable	77.84	-0.546
26.	PIK3C3	887	101487.33	6.28	119	112	117870-117120	42.30 Unstable	85.38	-0.434
27.	PIK3R4	1358	152598.92	6.68	158	151	156535-155160	48.96 Unstable	91.98	-0.249
28.	RB1CC1	1588	182349.94	5.35	269	208	75020-72770	51.75 Unstable	87.69	-0.560
29.	SQSTM1	442	48162.74	5.09	65	44	47160-46410	54.23 Unstable	60.50	-0.646
30.	TUFM	452	49508.35	7.23	57	57	26275-25900	40.07 Unstable	94.47	-0.179
31.	UVRAG	698	77524.94	8.20	82	86	45810-44810	54.44 Unstable	83.44	-0.477
32.	WDFY3	3508	392337.93	6.35	383	347	387060-382060	49.78 Unstable	89.23	-0.187
33.	WIPI2	445	48477.14	5.58	50	41	28725-27850	35.56 Stable	84.22	-0.120
34.	NOD2	1035	115300.92	6.84	104	100	93330-91330	49.69 Unstable	103.90	0.009

*GRAVY-Grand average of hydropathicity- Sum of hydropathy values of all amino acid divided by protein length. AA-Amino acid
*Theoretical PI- Isoelectric Point; *M.W- Molecular Weight

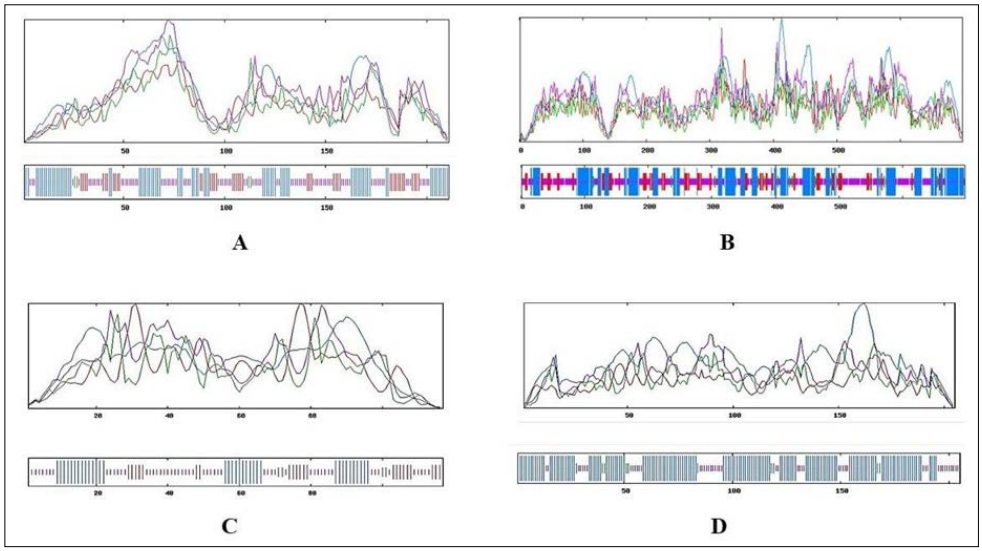

Figure 2: (A) Secondary Structure of ATG3 (B) Secondary Structure of ATG16L1 (C) Secondary Structure of ATG12 (D) Secondary Structure of TECPR1

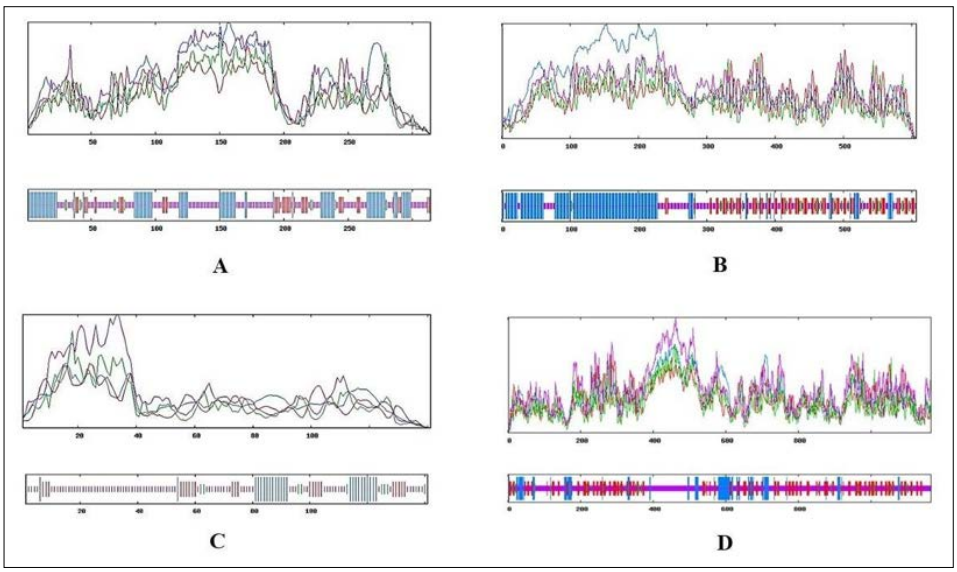

Figure 3: (A) Secondary Structure of ATG10 (B) Secondary Structure of ATG7 (C) Secondary Structure of GABARAP (D) Secondary Structure of FADD

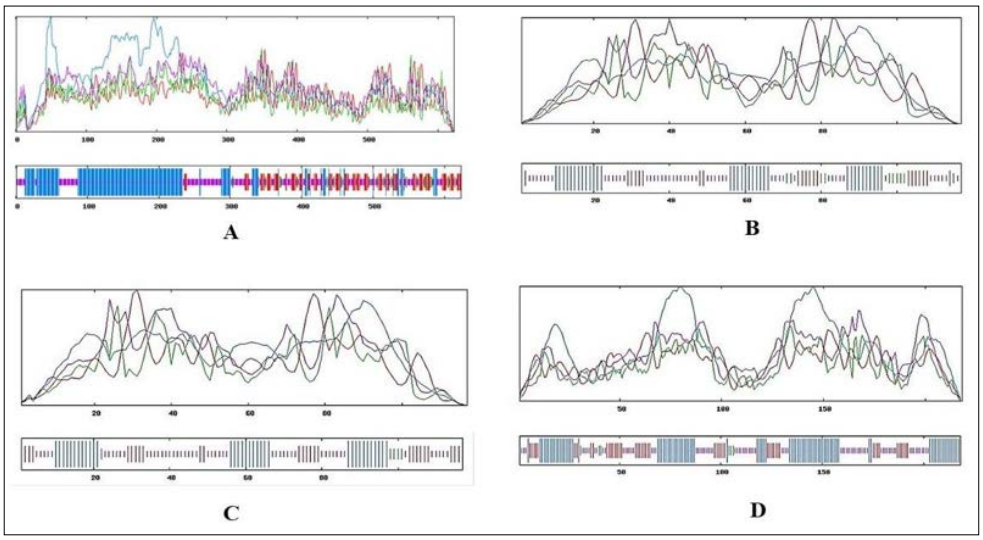

Figure 4: (A) Secondary Structure of ATG16L2 (B) Secondary Structure of GABARAPL1 (C) Secondary Structure of MAP1LC3B (D) Secondary Structure of MAP1LC3A

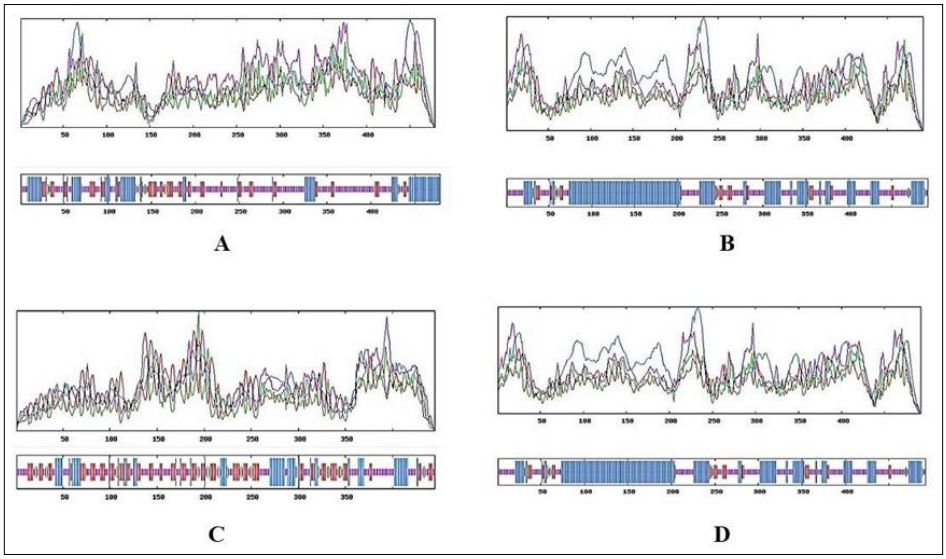

Figure 5: (A) Secondary Structure of PIK3C3 (B) Secondary Structure of BCL2L1 (C) Secondary Structure of WIPI2 (D) Secondary Structure of BECN1

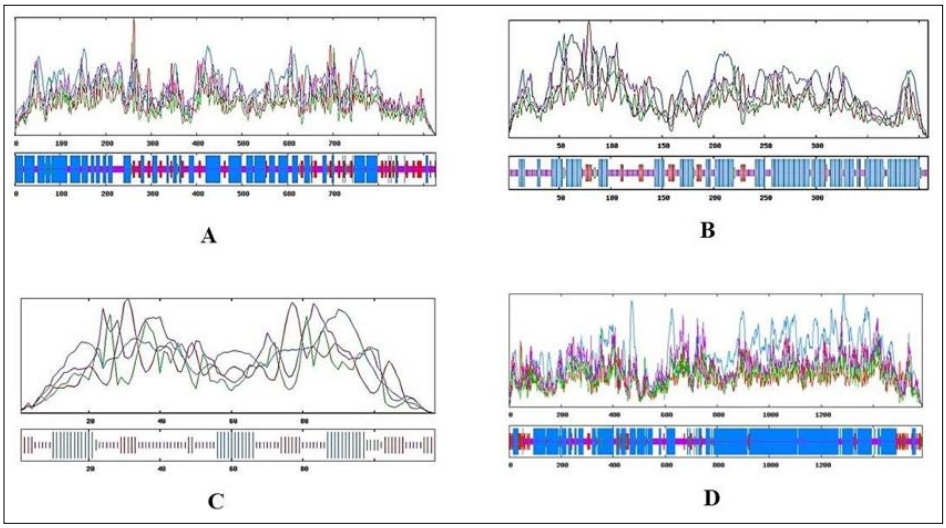

Figure 6: (A) Secondary Structure of DDX58 (B) Secondary Structure of IRGM1 (C) Secondary Structure of GABARAPL2 (D) Secondary Structure of RB1CC1

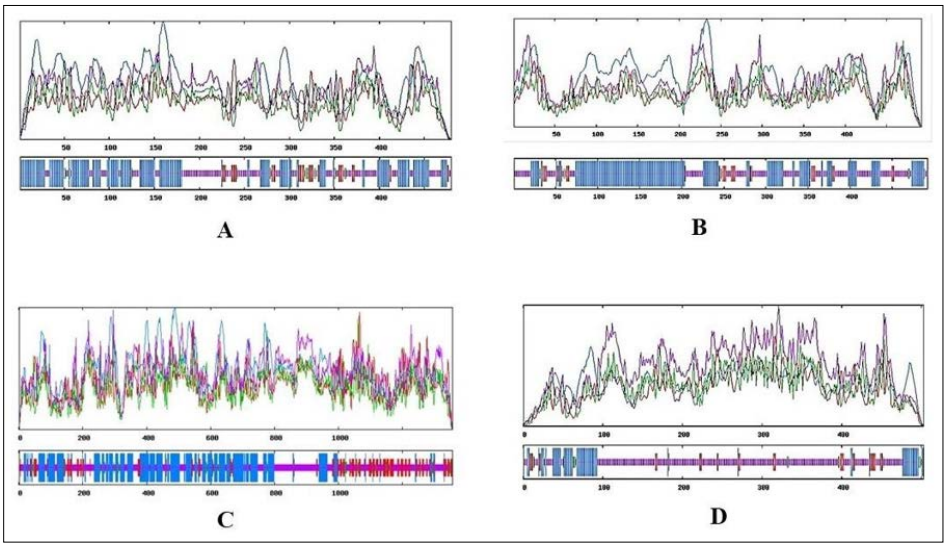

Figure 7: (A) Secondary Structure of CASP8 (B) Secondary Structure of ATG14 (C) Secondary Structure of PIK3R4 (D) Secondary Structure of MAVS

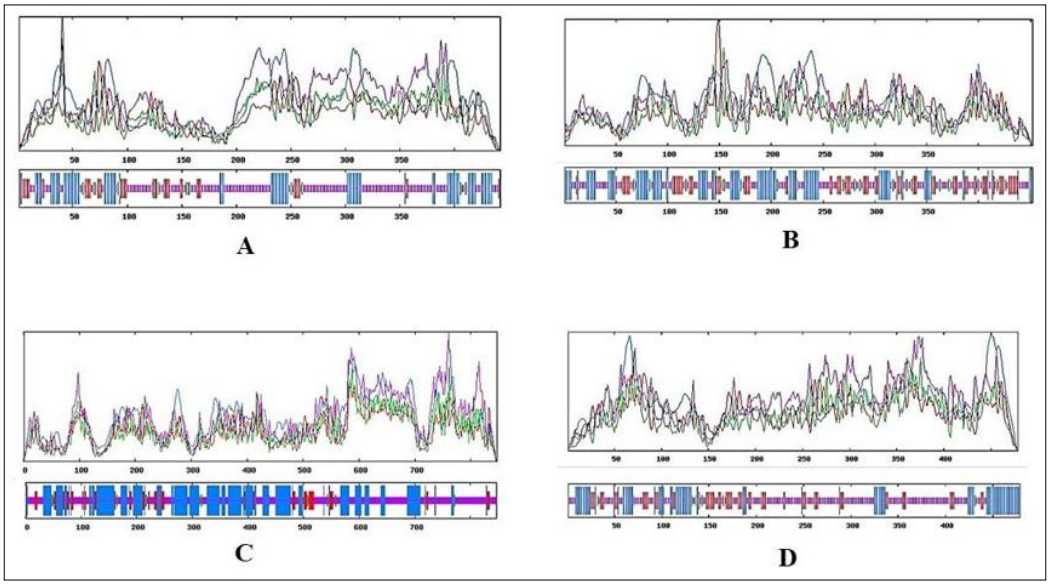

Figure 8: (A) Secondary Structure of SQSTM1 (B) Secondary Structure of TUFM (C) Secondary Structure of ATG9A (D) Secondary Structure of ATG13

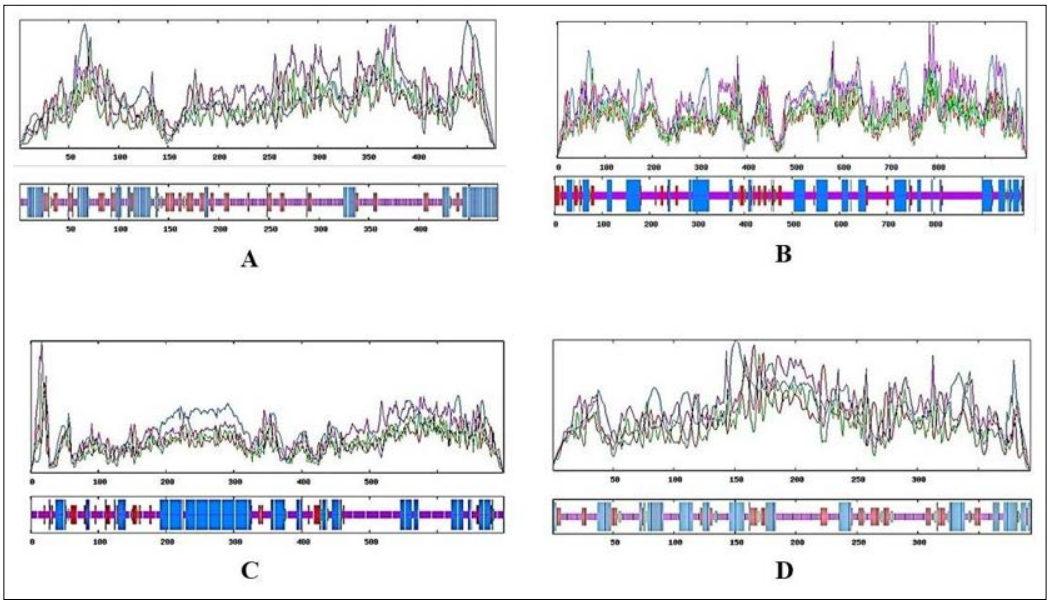

Figure 9: (A) Secondary Structure of WDFY3 (B) Secondary Structure of NBR1 (C) Secondary Structure of UVRAG (D) Secondary Structure of ATG4B

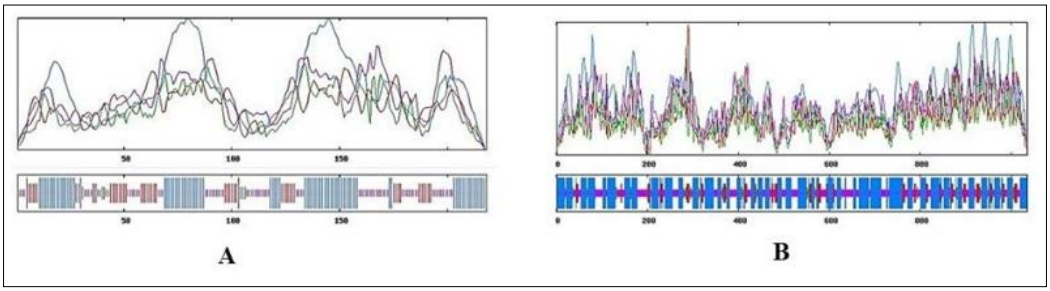

Figure 10: (A) Secondary Structure of ATG101 (B) Secondary Structure of NOD2

Table 3: Amino Acid Composition of ATG5 Interacting Proteins

S.N.	Amino Acid(%)	A (Ala)	R (Arg)	N (Asn)	D (Asp)	C (Cys)	Q (Gln)	E (Glu)	G (Gly)	H (His)	I (lle)	L (Leu)	K (Lys)	M (Met)	F (Phe)	P (Pro)	S (Ser)	T (Thr)	W (Trp)	Y (Tyr)	V (Val)
	Protein																				
1.	ATG3	6.4	2.2	1.6	7.3	2.5	3.5	12.4	5.7	3.8	5.7	7.6	7.3	2.5	2.2	4.5	2.5	8.6	1.3	5.1	7.0
2.	ATG16L1	8.3	6.9	3.2	7.2	1.3	4.8	7.7	5.1	2.9	4.3	10.4	6.3	1.6	2.7	2.9	9.3	5.5	1.8	1.3	6.4
3.	ATG12	7.1	1.4	0.7	5.0	1.4	4.3	8.5	7.8	0.7	5.0	9.2	8.5	1.4	3.5	9.2	9.2	6.4	1.4	2.1	7.1
4.	TECPR1	6.3	6.0	3.1	5.2	2.5	4.0	6.3	9.0	2.4	2.9	6.4	4.2	1.5	2.4	6.3	9.6	5.3	5.0	3.2	8.5
5.	ATG10	5.2	3.8	3.8	3.8	3.3	5.2	9.0	4.7	3.8	4.3	9.5	4.7	1.9	4.7	6.2	6.6	6.2	2.4	4.3	6.6
6.	ATG7	8.2	4.6	3.7	6.4	2.9	3.7	4.9	6.7	2.4	3.0	12.3	5.3	2.7	5.2	6.0	6.3	4.7	1.4	2.7	6.7
7.	GABARAP	5.1	6.8	1.7	6.0	0.0	2.6	9.4	4.3	3.4	6.0	7.7	10.3	1.7	7.7	6.0	4.3	2.6	0.0	6.8	7.7
8.	FADD	7.3	8.8	3.4	6.8	1.5	2.4	9.8	4.9	1.5	1.0	16.1	6.3	2.0	2.4	2.9	9.8	3.4	1.0	0.5	8.3
9.	ATG16L2	10.2	7.5	3.2	5.1	2.6	7.1	6.9	5.6	2.9	3.0	10.0	5.6	0.3	2.1	3.4	8.2	4.7	1.9	1.6	8.0
10.	GABARAPL1	4.3	6.8	2.6	7.7	0.0	2.6	8.5	3.4	2.6	4.3	6.8	11.1	1.7	6.8	7.7	3.4	3.4	0.0	8.5	7.7
11.	MAP1LC3B	4.0	8.0	3.2	4.0	0.0	5.6	9.6	3.2	2.4	6.4	8.0	6.4	4.0	5.6	4.8	7.2	4.8	0.0	3.2	9.6
12.	MAP1LC3A	3.3	7.4	2.5	6.6	0.8	8.3	6.6	2.5	2.5	6.6	7.4	7.4	3.3	6.6	6.6	6.6	3.3	0.0	3.3	8.3
13.	PIK3C3	5.3	4.7	3.6	6.7	1.4	5.1	6.8	4.8	2.0	4.1	11.6	7.9	3.0	3.6	5.2	7.1	5.1	1.2	4.3	6.5
14.	BCL2L1	9.0	6.4	5.2	4.7	0.4	4.3	9.0	7.3	1.7	2.6	8.2	2.6	2.1	5.6	3.0	9.9	4.7	3.0	2.6	7.7
15.	WIPI	9.2	4.5	4.3	4.9	3.1	3.1	6.3	6.7	2.0	4.9	10.1	4.7	2.5	4.0	4.5	9.2	6.5	0.2	3.4	5.6
16.	BECN1	5.1	5.1	4.9	5.4	2.0	7.1	11.4	5.4	1.3	3.1	10.9	6.5	2.5	4.7	2.7	6.7	6.0	1.6	2.5	5.1
17.	DDX58	7.1	4.8	4.8	5.2	2.7	4.9	9.3	4.1	2.3	6.8	9.2	8.7	1.8	4.6	3.8	6.2	4.2	1.1	2.8	5.7
18.	IRGM1	4.6	6.4	3.9	5.4	2.4	3.7	6.1	4.2	1.7	5.4	11.2	6.4	2.7	4.4	4.4	9.0	5.9	1.0	3.2	8.1
19.	GABARAPL2	4.3	5.1	0.9	6.8	0.9	4.3	7.7	4.3	1.7	7.7	6.0	10.3	3.4	6.0	4.3	7.7	3.4	1.7	4.3	9.4
20.	RB1CC1	6.0	4.7	4.0	5.4	2.3	6.5	11.5	2.0	2.8	4.6	12.2	8.4	3.0	3.0	3.1	7.9	5.0	0.4	1.4	5.5
21.	CASP8	3.5	5.2	4.6	7.9	3.5	4.0	9.6	4.6	1.9	5.0	11.5	8.3	2.7	4.8	3.8	8.1	3.8	0.4	3.1	3.8
22.	ATG14	6.1	6.9	4.5	6.1	2.2	4.3	7.7	5.7	2.4	4.3	8.9	7.3	2.2	2.2	4.5	10.2	5.3	1.4	2.4	5.3
23.	PIK3R4	7.3	5.4	3.7	5.5	1.7	5.0	6.1	4.8	3.0	6.0	10.6	5.7	2.1	3.6	5.5	8.0	5.2	1.4	2.5	6.9
24.	MAVS	9.3	4.6	3.8	3.2	1.6	5.2	5.6	5.6	1.6	2.4	9.5	3.2	1.4	2.4	10.3	13.7	7.4	0.8	2.0	6.6
25.	SQSTM1	6.6	5.2	2.5	5.7	2.9	3.2	9.0	8.8	2.9	2.7	7.9	4.8	2.3	3.2	10.0	10.4	4.3	1.4	2.0	4.3
26.	TUFM	8.2	5.8	2.4	4.9	1.5	2.4	7.7	8.6	3.1	5.1	10.6	6.9	2.7	2.4	6.2	3.5	6.6	0.4	2.2	8.6
27.	ATG9A	7.6	6.3	2.6	3.0	2.0	5.5	6.8	7.0	3.9	5.0	11.8	2.5	1.7	5.3	6.3	7.4	4.5	1.8	3.0	6.1
28.	ATG13	5.8	4.2	2.7	6.1	1.7	3.3	7.3	6.3	2.7	4.8	8.4	4.6	3.1	4.6	7.1	10.6	7.1	0.4	2.3	6.9
29.	WDFY3	6.5	5.2	3.9	4.3	2.3	4.6	6.6	5.7	3.1	4.4	11.5	4.7	2.2	4.3	5.3	8.8	5.5	1.3	2.7	7.1
30.	NBR1	6.2	4.7	3.3	4.8	2.1	6.0	10.2	5.1	2.6	3.6	9.6	5.3	1.7	2.7	7.7	9.2	5.4	1.0	1.9	6.9
31.	UVRAG	6.9	6.0	4.7	4.7	2.3	5.3	7.0	7.2	2.9	4.3	11.6	6.3	1.0	3.6	5.4	8.7	3.9	0.4	2.7	5.0
32.	ATG4B	6.6	5.6	3.1	6.6	3.1	4.3	6.9	6.9	2.5	4.8	9.9	3.1	2.5	5.6	5.6	6.6	5.3	2.3	2.8	5.9
33.	ATG101	3.7	6.4	1.8	5.5	2.3	4.1	9.6	6.0	2.3	5.0	8.7	6.9	2.8	3.7	2.3	6.4	6.9	1.4	3.2	11.0
34.	NOD2	8.6	6.4	3.2	4.1	3.2	5.8	6.8	6.2	3.5	3.2	17.6	3.3	1.2	4.6	3.4	8.0	4.2	1.2	1.6	4.9

Table 4: Percentage Content of Different Secondary Structure of ATG5 Interacting Proteins

	Content of Secondary structure (%)				
S.N.	**Protein**	**α-Helix**	**β-Turn**	**Extended Strand**	**Random Coil**
1.	ATG3	31.53	4.14	14.65	49.68
2.	ATG16L1	39.87	7.25	21.42	31.47
3.	ATG12	17.73	6.38	15.60	60.28
4.	TECPR1	12.5	5.32	25.04	57.12
5.	ATG10	36.97	1.90	19.91	41.23
6.	ATG7	37.25	4.30	15.33	43.12
7.	GABARAP	31.62	3.42	18.80	46.15
8.	FADD	70.7	4.88	0.00	24.39
9.	ATG16L2	39.81	6.58	19.58	34.03
10.	GABARAPL1	29.06	8.55	19.66	42.74
11.	MAP1LC3B	32.00	5.60	14.40	48.00
12.	MAP1LC3A	33.06	8.26	16.53	42.15
13.	PIK3C3	40.59	4.85	14.54	40.02
14.	BCL2L1	49.79	6.44	7.73	36.05
15.	WIPI	17.08	6.74	29.21	46.97
16.	BECN1	51.56	2.68	10.71	35.04
17.	DDX58	51.84	3.24	12.10	32.83
18.	IRGM1	55.01	2.93	7.33	34.72
19.	GABARAPL2	30.77	4.27	21.37	43.59
20.	RB1CC1	68.70	3.72	7.30	20.28
21.	CASP8	48.54	3.33	8.12	40.00
22.	ATG14	49.80	2.03	7.72	40.45
23.	PIK3R4	39.62	3.61	15.24	41.53
24.	MAVS	16.50	3.18	7.55	72.76
25.	SQSTM1	25.11	4.98	10.86	59.05
26.	TUFM	30.75	8.85	21.90	38.50
27.	ATG9A	43.21	2.95	9.56	44.27
28.	ATG13	25.26	2.30	18.37	54.07
29.	WDFY3	43.58	3.67	10.7	42.01
30.	NBR1	30.57	2.63	9.92	56.88
31.	UVRAG	41.40	0.00	0.00	46.70
32.	ATG4B	29.26	5.09	17.30	48.35
33.	ATG101	39.91	2.75	22.02	35.32
34.	NOD2	53.91	5.12	9.86	31.11

Table 5: Functional Characterisation of ATG5 Interacting Proteins

S.N	Interactive Protein	N Terminal	Trans-membrane region	C Terminal	Type	Length	Characters
1.	ATG10	-	-	-	-	-	Soluble Protein
2.	ATG12	1	MSEDSEVVLQLPSAPVGA	18	Signal Peptide	18	Soluble Protein
3.	ATG16l1	-	-	-	-	-	Soluble Protein
4.	ATG16l2	-	-	-	-	-	Soluble Protein
5.	ATG3	-	-	-	-	-	Soluble Protein
6.	ATG7	-	-	-	-	-	Soluble Protein
7.	TECPR1	-	-	-	-	-	Soluble Protein
8.	FADD	1	MDPFLVLLHSLSGSLS	16	Signal Peptide	16	Soluble Protein
9.	GABARAP	-	-	-		-	Soluble Protein
10.	GABARAPl1	-	-	-		-	Soluble Protein
11.	MAP1LC3B						Soluble Protein
12.	MAP1LC3A	-	-	-	-	-	Soluble Protein
13.	PIK3C3	-	-	-	-	-	Soluble Protein
14.	BCL2L1	-	-	-	-	-	Soluble Protein
15.	WIPI2	-	-	-	-	-	Soluble Protein
16.	BECN1	-	-	-	-	-	Soluble Protein
17.	DDX58	-	-	-	-	-	Soluble Protein
18.	IRGM1	-	-	-	-	-	Soluble Protein
19.	GABARAPL2	-	-	-	-	-	Soluble Protein
20.	RB1CC1	-	-	-	-	-	Soluble Protein
21.	CASP8	1	MDFQSCLYAIAEELGSEDLAALKFLCLD		Signal Peptide	28	Soluble Protein
22.	ATG14	-	-	-	-	-	Soluble Protein
23.	PIK3R4	-	-	-	-	-	Soluble Protein
24.	MAVS	17 476	SKFCCVDVLEILPYLSCLTASD WAKWLGATSALLAVFLAVMLYR	38 497	Secondary Primary	22 22	Membrane Protein
25.	SQSTM1	-	-	-	-	-	Soluble Protein
26.	TUFM	-	-	-	-	-	Soluble Protein
27.	ATG9A	59 127 284 369	EMFELMQFLFVVAFTTFLVSCVD TILVIAGVFWIHRLIKFIYNICC LWIGIANFLLCPLILIWQILYAF LAKNGAFFAGSILAVLIALTIYD	81 149 306 391	Secondary Primary Primary Secondary	23 23 23 23	Membrane Protein
28.	ATG13	1	METELSSQDRKDLDKFIKFFALKTVQVIVQA	31	Signal Peptide	31	Soluble Protein
29.	WDFY3	-	-	-	-	-	Soluble Protein
30.	NBR1	-	-	-	-	-	Soluble Protein
31.	UVRAG	-	-	-	-	-	Soluble Protein
32.	ATG4B	-	-	-	-	-	Soluble Protein
33.	ATG101	-	-	-	-	-	Soluble Protein
34.	NOD2	1	MCSQEEFQAQRSQLVALLISGSLE	24	Signal Peptide	24	Soluble Protein

Table 6: Total Motifs and Domain Families of ATG5 Interacting Proteins

	Proteins	Prosite Pattern	Prosite Profile	pFam	Total Motifs
1.	ATG3	0	0	2	5
2.	ATG16l1	1	2	7	64
3.	ATG12	0	0	2	7
4.	Tecpr1	0	1	4	19
5.	ATG10	0	0	2	3
6.	ATG7	0	0	3	28
7.	GABARAP	0	0	2	19
8.	FADD	0	2	2	36
9.	ATG16l2	1	2	7	121
10.	GABARAPL1	0	0	3	24
11.	MAP1LC3B	0	0	3	17

12.	MAP1LC3A	0	0	2	17
13.	PIK3C3	2	3	4	51
14.	BCL2L1	4	2	3	16
15.	WIPI2	0	0	2	7
16.	BECN1	0	0	8	66
17.	DDX58	0	3	10	95
18.	IRGM1	0	1	5	14
19.	GABARAPL2	0	0	2	17
20.	RB1CC1	0	0	3	108
21.	CASP8	2	3	3	28
22.	ATG14	0	0	4	21
23.	PIK3R4	2	4	8	196
24.	MAVS	0	0	1	8
25.	SQSTM1	1	3	4	34
26.	TUFM	1	1	6	97
27.	ATG9A	0	0	3	11
28.	ATG13	0	0	1	3
29.	WDFY3	1	5	8	74
30.	NBR1	1	3	5	39
31.	UVRAG	0	1	3	22
32.	ATG4B	0	0	2	3
33.	ATG101	0	0	1	2
34.	NOD2	1	2	16	53

Table 7: ATG5 Interacting Protein Prosite Pattern Motifs

S.N.	Proteins	Motifs	Description
1.	ATG3	0	-
2.	ATG16L1	WD_REPEATS_1	PS00678, Trp-Asp (WD) repeats signature.
3.	ATG12	0	-
4.	TECPR1	0	-
5.	ATG10	0	-
6.	ATG7	0	-
7.	GABARAP	0	-
8.	FADD	0	-
9.	ATG16L2	WD_REPEATS_1	PS00678, Trp-Asp (WD) repeats signature.
10.	GABARAPL1	0	
11.	MAP1LC3B	0	
12.	MAP1LC3A	0	
13.	PIK3C3	PI3_4_KINASE_2	PS00916, Phosphatidylinositol 3- and 4-kinases signature 2.
		PI3_4_KINASE_1	PS00916, Phosphatidylinositol 3- and 4-kinases signature 2.
14.	BCL2L1	BH4_1	PS01260, Apoptosis regulator, Bcl-2 family BH4 motif signature.
		BH1	PS01080, Apoptosis regulator, Bcl-2 family BH1 motif signature.
		BH3	PS01259, Apoptosis regulator, Bcl-2 family BH3 motif signature.
		BH2	PS01258, Apoptosis regulator, Bcl-2 family BH2 motif signature.
15.	WIPI2	0	-
16.	BECN1	0	-
17.	DDX58	0	-
18.	IRGM1	0	-
19.	GABARAPL2	0	-
20.	RB1CC1	0	-

21.	CASP8	CASPASE_HIS	PS01121, Caspase family histidine active site.
		CASPASE_CYS	PS01122, Caspase family cysteine active site.
22.	ATG14	0	-
23.	PIK3R4	WD_REPEATS_1	PS00678, Trp-Asp (WD) repeats signature.
		PROTEIN_KINASE_ST	PS00108, Serine/Threonine protein kinases active-site signature.
24.	MAVS	0	-
25.	SQSTM1	ZF_ZZ_1	PS01357, Zinc finger ZZ-type signature.
26.	TUFM	G_TR_1	PS00301, Translational (tr)-type guanine nucleotide-binding (G) domain signature.
27.	ATG9A	0	-
28.	ATG13	0	-
29.	WDFY3	WD_REPEATS_1	PS00678, Trp-Asp (WD) repeats signature.
30.	NBR1	ZF_ZZ_1	PS01357, Zinc finger ZZ-type signature.
31.	UVRAG	0	-
32.	ATG4B	0	-
33.	ATG101	0	-
34.	NOD2	TATD_1	PS01137, TatD deoxyribonuclease family signature 1.

Table 8: ATG5 Interacting Proteins Prosite Profile Motifs

S.N.	Proteins	Motifs	Description
1.	ATG3	0	-
2.	ATG16L1	WD_REPEATS_REGION	PS50294, Trp-Asp (WD) repeats circular profile.
		WD_REPEATS_2	PS50082, Trp-Asp (WD) repeats profile.
3.	ATG12	0	-
4.	TECPR1	RICIN_B_LECTIN	PS50231, Lectin domain of ricin B chain profile.
5.	ATG10	0	-
6.	ATG7	0	-
7.	GABARAP	0	-
8.	FADD	DED	PS50168, Death effector domain (DED) profile.
		DEATH_DOMAIN	PS50017, Death domain profile.
9	ATG16L2	WD_REPEATS_REGION	PS50294, Trp-Asp (WD) repeats circular profile.
		WD_REPEATS_2	PS50082, Trp-Asp (WD) repeats profile.
10.	GABARAPL1	0	-
11.	MAP1LC3B	0	-
12.	MAP1LC3A	0	-
13.	PIK3C3	PI3_4_KINASE_3	PS50290, Phosphatidylinositol 3- and 4-kinases catalytic domain profile.
		C2_PI3K	PS51547, C2 phosphatidylinositol 3-kinase (PI3K)-type domain profile.
		PIK_HELICAL	PS51545, PIK helical domain profile.
14.	BCL2L1	BCL2_FAMILY	PS50062, BCL2-like apoptosis inhibitors family profile.
		BH4_2	PS50063, Apoptosis regulator, Bcl-2 family BH4 motif profile.
15.	WIPI2	0	-
16.	BECN1	0	-
17.	DDX58	RLR_CTR	PS51789, RIG-I-like receptor (RLR) C-terminal regulatory (CTR) domain profile.
		HELICASE_ATP_BIND_1	PS51192, Superfamilies 1 and 2 helicase ATP-binding type-1 domain profile.
		HELICASE_CTER	PS51194, Superfamilies 1 and 2 helicase C-terminal domain profile.

18.	IRGM1	G_IRG	PS51716, IRG-type guanine nucleotide-binding (G) domain profile.
19.	GABARAPL2	0	-
20.	RB1CC1	0	-
21.	CASP8	CASPASE_P20	PS50208, Caspase family p20 domain profile.
		CASPASE_P10	PS50207, Caspase family p10 domain profile.
		DED	PS50168, Death effector domain (DED) profile.
22.	ATG14	0	-
23.	PIK3R4	PROTEIN_KINASE_DOM	PS50011, Protein kinase domain profile.
		WD_REPEATS_REGION	PS50294, Trp-Asp (WD) repeats circular profile.
		WD_REPEATS_2	PS50082, Trp-Asp (WD) repeats profile.
		HEAT_REPEAT	PS50077, HEAT repeat profile.
24.	MAVS	0	-
25.	SQSTM1	PB1	PS51745, PB1 domain profile.
		ZF_ZZ_2	PS50135, Zinc finger ZZ-type profile.
		UBA	PS50030, Ubiquitin-associated domain (UBA) profile.
26.	TUFM	G_TR_2	PS51722, Translational (tr)-type guanine nucleotide-binding (G) domain profile.
27.	ATG9A	0	-
28.	ATG13	0	-
29.	WDFY3	BEACH	PS50197, BEACH domain profile.
		PH_BEACH	PS51783, BEACH-type PH domain profile.
		ZF_FYVE	PS50178, Zinc finger FYVE/FYVE-related type profile.
		WD_REPEATS_REGION	PS50294, Trp-Asp (WD) repeats circular profile.
		WD_REPEATS_2	PS50082, Trp-Asp (WD) repeats profile.
30.	NBR1	PB1	PS51745, PB1 domain profile.
		ZF_ZZ_2	PS50135, Zinc finger ZZ-type profile.
		UBA	PS50030, Ubiquitin-associated domain (UBA) profile.
31.	UVRAG	C2	PS50004, C2 domain profile.
32.	ATG4B	0	-
33.	ATG101	0	-
34.	NOD2	NACHT	PS50837, NACHT-NTPase domain profile.
		CARD	PS50209, CARD caspase recruitment domain profile.

Table 9: ATG5 Interacting Proteins pFAM Domain Families

S.N.	Proteins	pFAM	Description
1.	ATG3	Autophagy_act_C	PF03987, Autophagocytosis associated protein, active-site domain
		SDA1	PF05285, SDA1
2.	ATG16L1	ATG16	PF08614, Autophagy protein 16 (ATG16)
		WD40	PF00400, WD domain, G-beta repeat
		ANAPC4_WD40	PF12894, Anaphase-promoting complex subunit 4 WD40 domain
		eIF2A	PF08662, Eukaryotic translation initiation factor eIF2A
		NBCH_WD40	PF20426, Neurobeachin beta propeller domain
		KASH_CCD	PF14662, Coiled-coil region of CCDC155 or KASH
		TolB_like	PF15869, TolB-like 6-blade propeller-like
3.	ATG12	APG12	PF04110, Ubiquitin-like autophagy protein Apg12
		ATG8	PF02991, Autophagy protein Atg8 ubiquitin like
4.	TECPR1	Hyd_WA	PF06462, Propeller
		Tectonin	PF19193, Tectonin domain
		Pex24p	PF06398, Integral peroxisomal membrane peroxin

		PH	PF00169, PH domain
5.	ATG10	Autophagy_act_C	PF03987, Autophagocytosis associated protein, active-site domain
		Zinc_ribbon_4	PF13717, zinc-ribbon domain
6.	ATG7	ATG7_N	PF16420, Ubiquitin-like modifier-activating enzyme ATG7 N-terminus
		ThiF	PF00899, ThiF family
		Shikimate_DH	PF01488, Shikimate / quinate 5-dehydrogenase
7.	GABARAP	ATG8 APG12	PF02991, Autophagy protein Atg8 ubiquitin like PF04110, Ubiquitin-like autophagy protein Apg12
		APG12	PF04110, Ubiquitin-like autophagy protein Apg12
8.	FADD	DED	PF01335, Death effector domain
		Death	PF00531, Death domain
9.	ATG16L2	ATG16	PF08614, Autophagy protein 16 (ATG16)
		WD40	PF00400, WD domain, G-beta repeat
		NBCH_WD40	PF20426, Neurobeachin beta propeller domain
		IFT57	PF10498, Intra-flagellar transport protein 57
		TerY_C	PF15616, TerY-C metal binding domain
		TFIIA	PF03153, Transcription factor IIA, alpha/beta subunit
		P4Ha_N	PF08336, Prolyl 4-Hydroxylase alpha-subunit, N-terminal region
10.	GABARAPL1	ATG8	PF02991, Autophagy protein Atg8 ubiquitin like
		APG12	PF04110, Ubiquitin-like autophagy protein Apg12
		VitD-bind_III	PF09164, Vitamin D binding protein, domain III
11.	MAP1LC3B	ATG8	PF02991, Autophagy protein Atg8 ubiquitin like
		APG12	PF04110, Ubiquitin-like autophagy protein Apg12
		Rad60-SLD	PF11976, Ubiquitin-2 like Rad60 SUMO-like
12.	MAP1LC3A	ATG8	PF02991, Autophagy protein Atg8 ubiquitin like
		APG12	PF04110, Ubiquitin-like autophagy protein Apg12
13.	PIK3C3	PI3Ka	PF00613, Phosphoinositide 3-kinase family, accessory domain (PIK domain)
		PI3_PI4_kinase	PF00454, Phosphatidylinositol 3- and 4-kinase
		PI3K_C2	PF00792, Phosphoinositide 3-kinase C2
		HEAT_2	PF13646, HEAT repeats
14.	BCL2L1	Bcl-2	PF00452, Apoptosis regulator proteins, Bcl-2 family
		BH4	PF02180, Bcl-2 homology region 4
		Bcl-2_3	PF15286, Apoptosis regulator M11, B cell 2 leukaemia/lymphoma like
15.	WIPI2	ANAPC4_WD40	PF12894, Anaphase-promoting complex subunit 4 WD40 domain
		VID27	PF08553, VID27 C-terminal WD40-like domain
16.	BECN1	APG6	PF04111, Apg6 BARA domain
		APG6_N	PF17675, Apg6 coiled-coil region
		BH3	PF15285, Beclin-1 BH3 domain, Bcl-2-interacting
		MT	PF12777, Microtubule-binding stalk of dynein motor
17.	DDX58	CARD_2	PF16739, Caspase recruitment domain
		RIG-I_C	PF18119, RIG-I receptor C-terminal domain
		RIG-I_C-RD	PF11648, C-terminal domain of RIG-I
		Helicase_C	PF00271, Helicase conserved C-terminal domain
		ResIII	PF04851, Type III restriction enzyme, res subunit
		DEAD	PF00270, DEAD/DEAH box helicase
		AAA_25	PF13481, AAA domain
		AAA_22	PF13401, AAA domain
		ApoLp-III	PF07464, Apolipophorin-III precursor (apoLp-III)
		ATP-synt_ab	PF00006, ATP synthase alpha/beta family, nucleotide-binding domain

18.	IRGM1	IIGP	PF05049, Interferon-inducible GTPase (IIGP)
		MMR_HSR1	PF01926, 50S ribosome-binding GTPase
		Dynamin_N	PF00350, Dynamin family
		RsgA_GTPase	PF03193, RsgA GTPase
		LYTB	PF02401, LytB protein
19.	GABARAPL2	ATG8	PF02991, Autophagy protein Atg8 ubiquitin like
		APG12	PF04110, Ubiquitin-like autophagy protein Apg12
20.	RB1CC1	ATG11	PF10377, Autophagy-related protein 11
		ATG17_like	PF04108, Autophagy protein ATG17-like domain
		TBK1_ULD	PF18396, TANK binding kinase 1 ubiquitin-like domain
21.	CASP8	DED	PF01335, Death effector domain
		Peptidase_C14	PF00656, Caspase domain
		PYRIN	PF02758, PAAD/DAPIN/Pyrin domain
22.	ATG14	ATG14	PF10186, Vacuolar sorting 38 and autophagy-related subunit 14
		Borrelia_P83	PF05262, Borrelia P83/100 protein
		MnmE_helical	PF12631, MnmE helical domain
		Exonuc_VII_L	PF02601, Exonuclease VII, large subunit
23.	PIK3R4	Pkinase	PF00069, Protein kinase domain
		WD40	PF00400, WD domain, G-beta repeat
		HEAT	PF02985, HEAT repeat
		PK_Tyr_Ser-Thr	PF07714, Protein tyrosine and serine/threonine kinase
		NBCH_WD40	PF20426, Neurobeachin beta propeller domain
		HEAT_2	PF13646, HEAT repeats
		IFRD	PF05004, Interferon-related developmental regulator (IFRD)
		TCAD9	PF19974, Ternary complex associated domain 9
24.	MAVS	CARD_2	PF16739, Caspase recruitment domain
25.	SQSTM1	UBA_5	PF16577, UBA domain
		PB1	PF00564, PB1 domain
		ZZ	PF00569, Zinc finger, ZZ type
		C1_2	PF03107, C1 domain
26.	TUFM	GTP_EFTU	PF00009, Elongation factor Tu GTP binding domain
		GTP_EFTU_D3	PF03143, Elongation factor Tu C-terminal domain
		GTP_EFTU_D2	PF03144, Elongation factor Tu domain 2
		MMR_HSR1	PF01926, 50S ribosome-binding GTPase
		RsgA_GTPase	PF03193, RsgA GTPase
		DO-GTPase2	PF19993, Double-GTPase 2
27.	ATG9A	ATG9	PF04109, Autophagy protein ATG9
		Saf_2TM	PF18303, SAVED-fused 2TM effector domain
		PRRSV_2b	PF07069, Porcine reproductive and respiratory syndrome virus 2b
28.	ATG13	ATG13	PF10033, Autophagy-related protein 13
29.	WDFY3	Beach	PF02138, Beige/BEACH domain
		FYVE	PF01363, FYVE zinc finger
		PH_BEACH	PF14844, PH domain associated with Beige/BEACH
		NBCH_WD40	PF20426, Neurobeachin beta propeller domain
		WD40	PF00400, WD domain, G-beta repeat
		DUF4704	PF15787, Neurobeachin/BDCP, DUF4704 alpha solenoid region
		Laminin_G_3	PF13385, Concanavalin A-like lectin/glucanases superfamily
		DUF4800	PF16057, Domain of unknown function (DUF4800)

30.	NBR1	N_BRCA1_IG	PF16158, Ig-like domain from next to BRCA1 gene
		PB1	PF00564, PB1 domain
		ZZ	PF00569, Zinc finger, ZZ type
		Knl1_RWD_C	PF18210, Knl1 RWD C-terminal domain
		C1_2	PF03107, C1 domain
31.	UVRAG	ATG14	PF10186, Vacuolar sorting 38 and autophagy-related subunit 14
		VPS38	PF17649, Vacuolar protein sorting 38
		C2	PF00168, C2 domain
32.	ATG4B	Peptidase_C54	PF03416, Peptidase family C54
		ATG4_LIR	PF20166, ATG4, F-type LIR motif
33.	ATG101	ATG101	PF07855, Autophagy-related protein 101
34.	NOD2	ATG101	PF07855, Autophagy-related protein 101
		NACHT	PF05729, NACHT domain
		CARD	PF00619, Caspase recruitment domain
		LRR_6	PF13516, Leucine Rich repeat
		NLRC4_HD2	PF17776, NLRC4 helical domain HD2
		NOD2_WH	PF17779, NOD2 winged helix domain
		LRR_4	PF12799, Leucine Rich repeats (2 copies)
		AAA_29	PF13555, P-loop containing region of AAA domain
		AAA_22	PF13401, AAA domain
		AAA_16	PF13191, AAA ATPase domain
		AAA_25	PF13481, AAA domain
		AAA_30	PF13604, AAA domain
		NB-ARC	PF00931, NB-ARC domain
		AAA_33	PF13671, AAA domain
		ABC_tran	PF00005, ABC transporter
		G-alpha	PF00503, G-protein alpha subunit
		AAA_15	PF13175, AAA ATPase domain

Table 10: ATG5 Interacting Proteins Active Sites

Protein	AA Position	Description	Length
ATG3	264	Glycyl thioester intermediate	1
ATG10	165	Glycyl thioester intermediate	1
ATG7	567	Glycyl thioester intermediate	1
ATG4B	74 278 280	Nucleophile - -	1 1 1
PIK3C4	148	Proton Acceptor	1

Extinction Coefficient (EC)

Extinction coefficients are measured in units of M^{-1} cm^{-1}, at 280nm measured in water [14]. The calculated EC is in direct correlation with the cysteine, tryptophan and tyrosine content of ATG5 interacting proteins. WDFY3 showed highest extinction coefficient among ATG5 interacting proteins in range of 387060-382060 M^{-1} cm^{-1}. Two proteins viz.
MAP1LC3A and MAP1LC3B showed low EC value of 5960 M^{-1} cm^{-1} each (Table 2).

Instability Index (II)

The instability index is a way for determining whether a protein will remain stable under various cellular conditions. If instability index is lower than forty, then proteins are likely to remain stable and instability index higher than forty predicts unstable [15]. ExPASY tool predicted that the instability index of ATG5 interacting proteins showed five proteins namely: ATG7, GABARRAPL1, GABARAPL2, BCL2L1 and WIPI2 were stable in nature and remaining twenty-nine proteins namely: ATG3, ATG16L1, ATG12, TECPR1, ATG10, GABARAP, FADD, ATG16L2, ATG101, ATG12, ATG14, ATG4B, ATG9A, BECN1, CASP8, DDX58, IRGM1, MAP1LC3A, MAP1LC3B, MAVS, NBR1, PIK3C3, PIK3C4, RB1CC1, SQSTM1, TUFM, UVRAG, WDFY3 and NOD2 were unstable (Table 2).

Aliphatic Index

The relative volume filled by aliphatic side chains (alanine, valine, isoleucine and leucine) is defined as the aliphatic index of a protein [16]. It could be interpreted as a beneficial factor in favor of protein thermostability. Aliphatic index of ATG5 interacting proteins ranged from 60.50 to 103.90. ATG5 interacting protein SQSTM1 and Tecpr1 showed low thermal stability of 60.50 and 67.34 respectively. In contrast, NOD2 and FADD showed higher aliphatic index of 103.90 and 97.95 respectively. The remaining thirty interacting proteins ranged from 69.91 to 94.47 (Table 2).

GRAVY (Grand Average of Hydropathy)

The total hydropathy values of all the amino acids in a protein is divided by the number of aa residues to get the GRAVY value [17]. ATG5 interacting proteins showed negative GRAVY values which predicts its non-polar nature except NOD2 protein having positive GRAVY value of 0.009 indicating its polar nature (Table 2).

Amino acid composition of ATG5 interacting proteins were given in Table 3. ATG5 interacting proteins contain higher percentage of hydrophobic amino acid leucine and neutral amino acid serine. Also, low percentage of cysteine and histidine amino acids were predicted.

Secondary Structure Prediction

In this study, amino acids cysteine (C), tryptophan (W), methionine (M) and histidine (H) was found to be low in numbers among all thirty-four interacting proteins. This shows that these proteins cannot be analyzed using UV spectral methods [18]. The polypeptide backbone of local conformation proteins is referred to as secondary structure forming regular structures like α-helix, β-strand, random coils and extended strands. It is a critical step in predicting tertiary structure and gives crucial information about protein action [19]. ATG5 interacting proteins secondary structure predicted alpha helix and random coils were far more abundant than other secondary structures such as β-turn (Table 4, Figure 2-10).

Functional Characterisation

SOSUI server predicted functional characterisation of ATG5 interacting proteins (Table 5). ATG5 interacting proteins namely; ATG10, ATG16L1, ATG16L2, ATG3, ATG7, TECPR1, GABARAP, GABARAPL1, MAP1LC3B, MAP1LC3A, PIK3C3, BCL2L1, WIPI2, BECN1, DDX58, IRGM1, GABARAPL2, RB1CC1, ATG14, PIK3R4, SQSTM1, TUFM, WDFY3,NBR1, UVRAG, ATG4B and ATG101 were predicted as soluble protein. Moreover, ATG12 contains 1 Trans-membrane of length-18aa., FADD contains 1 Trans-membrane region of length-16aa., CASP8 contains 1 Trans-membrane region of length-28aa and ATG13 contains 1 Trans-membrane region of lengh-31aa, NOD2 showed 1 Trans-membrane region of length- 24aa. were predicted as signal peptides. There were two membrane proteins predicted of primary and secondary character namely: MAVS contains two transmembrane helices of length 23aa each and ATG9A having four transmembrane helices of length 23aa individually.

ATG5 Interacting Proteins Predicted Motifs and Families

In this study, out of thirty-four ATG5 interacting proteins, ten proteins namely; ATG16l2, PIK3C3, BCL2L1, CASP8, PIK3R4, SQSTM1, TUFM, WDFY3, NBR1 and NOD2 showed both Prosite Pattern and Prosite Profile. The maximum number of Prosite Pattern and Prosite Profile was found in BCL2L1 and WDFY3 respectively. Further, 3 proteins viz, Tecpr1, FADD, DDX58 showed only Prosite Profile. However, there were seventeen proteins namely; ATG3, ATG10, ATG7, GABARAP, GABARAPL1, MAP1LC3B, MAP1LC3A, WIPI2, BECN1, GABARAPL2, RB1CC1, ATG14, MAVS, ATG9A, ATG13, ATG4B and ATG101 showed no Prosite Pattern and Prosite Profile. pFAM shows accurate group of protein domains and families [20]. The current study showed NOD2 an ATG5 interacting with sixteen protein families which have highest among all (Table 6-9).

Prediction of Active Sites and Regions

After binding of substrate to an active site of an enzyme, catalysis or chemical reactions take place. When a protein undergoes an enzyme reaction, active sites act as a structural feature that determines functioning of protein. In this study, total of five ATG5 interacting proteins i.e., ATG3(Position of aa-264), ATG10(Position of aa-165), ATG4B (Position of aa-74,278,280), ATG7(Position of aa-567) and PIK3C4(Position-148) showed active sites of length one amino acid independently (Table 10). ATG3, ATG10, ATG7 actively binds glycyl thioester intermediate whereas ATG4B showed an active site for nucleophile binding whereas PIK3C4 for proton binding.

Discussion

In eukaryotes, autophagy is one of the main processes for proteins turnover. Few modulations in autophagy process may show diverse molecular functions of proteins. There is not enough full annotation for the genes and proteins involved in autophagy. Numerous genes implicated in autophagy might have different activities or be involved in different cellular processes. It is difficult to find appropriate biomarkers for autophagy and associated processes. Further, to track autophagic activity in cells and tissues, biomarkers are crucial. The assessment of autophagy in various experimental contexts is complicated by the absence of well recognised and validated indicators. However, these components attain a net change in cellular character. Therefore, it was critical to evaluate a protein's interactions with other proteins while investigating their function. ATG5 have been interacted with ATG1 and ATG18 which reverses oxidative stress triggered synapse overgrowth [21]. Nevertheless, along performing crucial protective function in many diseases, uncontrolled autophagy can lead to excessive degradation of cellular components causing cell death. ATG5 plays vital role for cell death function by interacting with FADD [22]. The complexities of neurological processes may be reduced by bioinformatics techniques. It is a continuous challenge to develop more complicated models that take into account the complex nature of neural circuits and connections. In numerous neurodegenerative disorders like Alzheimer's disease, Parkinson's disease, and amyotrophic lateral sclerosis, aggregation of misfolded proteins remains as marker. This accumulation directly disturbs basal neuronal autophagy level [23]. Further, ATG5 interacting protein ATG7 is an essential effector enzyme for autophagy function loss of which exhibit complex neurodevelopmental disorders like ataxia and developmental delay [24]. Taylor et al. reported that absence of ATG7 in muscles cells of human resulted in impaired LC3 lipidation and autophagy flux [25]. Demonstrated roles of ATG16l1 in neurogenesis and stem cell development which is one of the ATG5 interacting protein predicted in this study. Moreover, ATG5 interacting membrane protein ATG9A interacted with lipid droplets and involve in cell survival, mitochondrial maintenance and recovery of neurogenesis defects due to impaired autophagy. Depletion of ATG9 resulted in abnormal development of axon tracts in brain regions of mouse causing axon specific lesions [26].

The STRING database showed detailed study and integration of protein-protein interactions. The data shown in the prediction

of amino acids number where, Leu (L) and Ser (S) were found highest in interacting proteins and Cys (C), His (H), Met (M) and Trp (W) were found low in count (Table 3). Low levels of essential amino acids which are the precursors of various neurotransmitters may show deprived signal transduction in mice [27]. Disulfide covalent bridges formed by cysteine-cysteine residues have an important role in folding along with stability of proteins. This results from an oxidative folding method that takes place in thiol groups cysteines. Studies have suggested ways to make proteins more stable by mutating cysteine. Moreover, the stability decreases when the natural disulfide links are broken [28]. Hence, majority of ATG5 interacting proteins were unstable in nature as they lack cysteine-cysteine disulfide bridges. Leucine is a strong activator of the mechanistic target of rapamycin (mTOR) pathway that promotes anabolic cellular processes and growth which further ameliorate protein catabolism by autophagy mechanism [29]. Leucine also contributes to protein thermostability nonetheless, serine is investigated to be predominantly synthesized in astrocytes and not in neurons, indicating that it is an essential amino acid for neurons [30]. ATG5 interacting protein negative charges (-R) were calculated using the aspartic and glutamic acid content, while their positive charges (+R) were calculated using the arginine and lysine content by ExPASY ProtParam tool. According to Table 2, the majority of ATG interacting proteins showed pI values lower than 7, predicting aspartic and glutamic acids constitutes ATG5 interacting sequence than arginine and lysine. The ATG5 interacting proteins' aliphatic index ranged from 60.50 to 103.90. Therefore, proteins can maintain their stability in higher temperature range due to presence of high aliphatic index.

The secondary structures of proteins such as α-helical structure is composed of methionine(M), alanine (A), leucine (L), glutamate (E), and lysine (K) amino acids, whereas the electrostatic repulsion and steric hinderance between bulky side chains of isoleucine or charged side chains of glutamic and aspartic acid causes a protein to adopt a random coil conformation. The random coil is typically described as a folded chain area that is more flexible and dynamic than other secondary conformational structures [31]. β-strand are composed of tryptophan (W), tyrosine (Y), phenylalanine (F), valine (V), isoleucine (I) and threonine (T), furthermore, glycine (G) and proline (P) amino acids help to build the relevant turns [32]. The predicted findings suggest that the amino acids concentration is simply responsible for making the particular secondary structure of proteins. The percentage score of amino acid distribution of ATG5 interacting proteins concludes that α-helix and random coils were dominant over other secondary structures followed by β-strand and turns (Table 4) which supports the amino acid compositions.

Protein solubility is an important feature. Intrinsic parameters like amino acid sequence and non-intrinsic parameters like temperature, ionic strength and pH influence protein solubility [33]. Protein accumulation and folding in the cellular environment are incompatible with one another because overexpression of unfolded proteins causes inclusion bodies to form [34]. In addition, the given data suggested soluble signal peptides interacts with ATG5. These signal peptides attach with the N-terminus of desired protein that directs them to the periplasmic space and resolves improper folding and overexpression of protein [35]. Most of the ATG5 interacting proteins were hydrophobic in nature. There are various factors like hydrophobicity, protein molecules volume, electric charge responsible for protein stability. Hydrophobicity is one of the most important factors of transmembrane helices also ATG9A is a sole multispanning membranous protein responsible for the early phagophore expansion. It functions in the mobilization of lipid droplets to autophagosome and mitochondria, blocking of which leads to the inhibition of mitochondrial respiration and lipotoxicity [36]. The two transmembrane helices of the mitochondrial antiviral signaling (MAVS) protein have a significant function in antiviral and autoimmune responses. By directly attaching LIR motif to LC3, MAVS inhibits autophagy [37].

Conserved domains and families serve as a building block and can be recombined in different arrangements to make proteins with different functions, and often correspond to the 3D domains of a protein structure [38]. Protein domains and motifs can be computed using the prosite database. Prosite profile aims to characterize a family of protein or domain along with whole length as contrast to prosite pattern, which is restricted to a small region with strong sequence similarity [39]. Further, ATG5 interacting protein motifs, domains and families were assembled with respect to their common functionality. By closely observing the signature pattern of particular family it can be reliable to predict new proteins.

Protein-protein interaction (PPI) networks are used to locate the multiple molecular pathways and mechanisms that causes disorders. The closest interacting protein had the shortest node score of 0.999 namely: ATG16l1. It functions by interacting with ATG12-ATG5 to mediate the conjugation of phosphatidylethanolamine (PE) and activates LC3II. Protein structures are analyzed and their active sites are considered as the starting point for multiple PPI studies. In current study two interacting proteins namely: ATG4B and ATG9A showed catalytic activity. In addition, ATG5 interacting proteins like ATG3, ATG10 and ATG7 had active sites acting as glycyl thioester intermediate and ATG4B, PIK3C4 as nucleophile and proton acceptor respectively. PIK3R4 involved in initiation and maturation of autophagosomes and endocytosis predicted to have ATP binding site. The C-terminal lipidation of MAP1LC3 is mediated by ATG7, ATG3, ATG5 and ATG16L1, and their deletion reduces autophagy at the later or maturation stage of autophagosome production, resulting in a shortage of amino acids as well as rapid cell death within 24 h The conjugation of ATG3 occurs to LC3 to a lipid molecule, phosphatidylethanolamine (PE) on autophagosome membranes [40-46].

Conclusion

In the present study, ATG5 interacting proteins as represented in (Table 1), physicochemical and functional parameters were predicted using different computational tools. This study concludes that ATG5 interacting proteins were stable in higher temperature. Further, ATG5 interacting proteins were predicted to have higher percentage of α-helix and random coils. Furthermore, these proteins were predicted to be hydrophobic in nature. In addition, wet lab experiments are needed to confirm the binding of ATG5 with the in silico identified interacting proteins. This study provides limited information of the molecular mechanisms that control autophagy in higher eukaryotic cells. However, this study may be helpful to get a theoretical idea in developing certain biomolecules for autophagy. In conclusion, predicting different properties and binding sites may contribute a better understanding of ATG5 regulatory functions that may give potential target for docking studies.

References

1. Kim JH, Hong SB, Lee JK, Han S, Roh KH, et al. (2015) Insights into autophagosome maturation revealed by the structures of ATG5 with its interacting partners. Autophagy 11: 75-87.
2. Vellai T (2009) Autophagy genes and ageing. Cell Death Differ 16: 94-102.
3. Vij A, Randhawa R, Parkash J, Changotra H (2016) Investigating regulatory signatures of human autophagy related gene 5 (ATG5) through functional in silico analysis. Meta gene 9: 237-248.
4. Tang M, Liu T, Jiang P, Dang R (2021) the interaction between autophagy and neuroinflammation in major depressive disorder: From pathophysiology to therapeutic implications. Pharmacol Res 168: 105586.
5. Nishiyama J, Miura E, Mizushima N, Watanabe M, Yuzaki M (2007) Aberrant membranes and double-membrane structures accumulate in the axons of Atg5-null Purkinje cells before neuronal death. Autophagy 3: 591-596.
6. Rao VS, Srinivas K, Sujini GN, Kumar GN (2014) Protein-protein interaction detection: methods and analysis. Int J Proteomics 2014: 147648.
7. Namba T, Takabatake Y, Kimura T, Takahashi A, Yamamoto T, et al. (2014) Autophagic clearance of mitochondria in the kidney copes with metabolic acidosis. J Am Soc Nephrol 25: 2254-2266.
8. Collier JJ, Oláhová M, McWilliams TG, Taylor RW (2021) ATG7 safeguards human neural integrity. Autophagy 17: 2651-2653.
9. Kuma A, Hatano M, Matsui M, Yamamoto A, Nakaya H, et al. (2004) The role of autophagy during the early neonatal starvation period. Nature 432: 1032-1036.
10. Brandi V, Di Lella V, Marino M, Ascenzi P, Polticelli F (2018) A comprehensive in silico analysis of huntingtin and its interactome. J Biomol Struct Dyn 36: 3155-3171.
11. Paramanik V, Krishnan H, Thakur MK (2018) Estrogen receptor α- and β-interacting proteins contain consensus secondary structures: An in-silico study. Ann Neurosci 25: 1-10.
12. Kurrey K, Paramanik V (2018) Identification and physiochemical analysis of ERK interacting proteins using bio-computational tools. World J Neurosci 8: 303-313.
13. Ma Y, Liu Y, Cheng J (2018) Protein secondary structure prediction based on data partition and semi-random subspace method. Sci Rep 8: 9856.
14. Hilario EC, Stern A, Wang CH, Vargas YW, Morgan CJ, et al. (2017) An improved method of predicting extinction coefficients for the determination of protein concentration. PDA J Pharm Sci Technol 71: 127-135.
15. Hoda A, Tafaj M, Sallaku E (2021) In silico structural, functional and phylogenetic analyses of cellulase from ruminococcus albus. J Genet Eng Biotechnol 19: 58.
16. Chang KY, Yang JR (2013) Analysis and prediction of highly effective antiviral peptides based on random forests. PloS one 8: 70166.
17. Zhang Z, Chow SY, De Guzman R, Joh NH, Joubert MK, et al. (2022) A mass spectrometric characterization of light-induced modifications in therapeutic Proteins. J Pharm Sci 111: 1556-1564.
18. Roy S, Maheshwari N, Chauhan R, Sen NK, Sharma A (2011) Structure prediction and functional characterization of secondary metabolite proteins of Ocimum. Bioinformation 6: 315-319.
19. Hulo N, Bairoch A, Bulliard V, Cerutti L, De Castro E, et al. (2006) The PROSITE database. Nucleic Acids Res 34: 227-230.
20. Milton VJ, Jarrett HE, Gowers K, Chalak S, Briggs L, et al. (2011) Oxidative stress induces overgrowth of the Drosophila neuromuscular junction. Proc Natl Acad Sci USA 108: 17521-17526.
21. Pyo JO, Jang MH, Kwon YK, Lee HJ, Jun JI, et al. (2005) Essential roles of Atg5 and FADD in autophagic cell death: dissection of autophagic cell death into vacuole formation and cell death. J Biol Chem 280: 20722-20729.
22. Collier JJ, Suomi F, Oláhová M, McWilliams TG, Taylor RW (2021) Emerging roles of ATG7 in human health and disease. EMBO Mol Med 13: 14824.
23. Ciechanover A, Kwon YT (2015) Degradation of misfolded proteins in neurodegenerative diseases: therapeutic targets and strategies. Exp Mol Med 47: 147.
24. Wu X, Fleming A, Ricketts T, Pavel M, Virgin H, et al. (2016) Autophagy regulates notch degradation and modulates stem cell development and neurogenesis. Nat Commun 7: 10533.
25. Yamaguchi J, Suzuki C, Nanao T, Kakuta S, Ozawa K, et al. (2018) Atg9a deficiency causes axon-specific lesions including neuronal circuit dysgenesis. Autophagy 14: 764-777.
26. Sarafeddinov A, Arif A, Peters A, Fuchsbauer HL (2011) A novel transglutaminase substrate from Streptomyces mobaraensis inhibiting papain-like cysteine proteases. J Microbiol Biotechnol 21: 617-626.
27. Gao X, Dong X, Li X, Liu Z, Liu H (2020) Prediction of disulfide bond engineering sites using a machine learning method. Sci Rep 10: 10330.
28. De Bandt JP (2016) Leucine and mammalian target of rapamycin-dependent activation of muscle protein synthesis in aging. J Nutr 146: 2616S-2624S.
29. Santhoshkumar R, Yusuf A (2020) In silico structural modeling and analysis of physicochemical properties of curcumin synthase (CURS1, CURS2, and CURS3) proteins of Curcuma longa. J Genet Eng Biotechnol 18: 24.
30. Sanjaya RE, Putri KDA, Kurniati A, Rohman A, Puspaningsih NNT (2021) In silico characterization of the GH5-cellulase family from uncultured microorganisms: physicochemical and structural studies. J Genet Eng Biotechnol 19: 143.
31. Lopez MJ, Mohiuddin SS (2023) Biochemistry, essential amino acids. In StatPearls Treasure Island (FL) StatPearls.
32. Trevino SR, Scholtz JM, Pace CN (2007) Amino acid contribution to protein solubility: Asp, Glu, and Ser contribute more favorably than the other hydrophilic amino acids in RNase Sa. J Mol Biol 366: 449-460.
33. Nogalska A, D'Agostino C, Engel WK, Cacciottolo M, Asada S, et al. (2015) Activation of the unfolded protein response in sporadic inclusion-body myositis but not in hereditary GNE inclusion-body myopathy. J Neuropathol Exp Neurol 74: 538-546.
34. Juibari AD, Ramezani S, Rezadoust MH (2019) Bioinformatics analysis of various signal peptides for periplasmic expression of parathyroid hormone in E.coli. J Med Life 12: 184-191.
35. Mailler E, Guardia CM, Bai X, Jarnik M, Williamson CD, et al. (2021) The autophagy protein ATG9A enables lipid mobilization from lipid droplets. Nat Commun 12: 6750.
36. Cheng J, Liao Y, Xiao L, Wu R, Zhao S, et al. (2017) Autophagy regulates MAVS signaling activation in a phosphorylation-dependent manner in microglia. Cell Death Differ 24: 276-287.
37. Mooney C, Davey N, Martin AJ, Walsh I, Shields DC, et al. (2011) In silico protein motif discovery and structural

analysis. Methods Mol Biol 760: 341-353.

38. Sigrist CJ, Cerutti L, Hulo N, Gattiker A, Falquet L, et al. (2002) PROSITE: a documented database using patterns and profiles as motif descriptors. Brief Bioinform 3: 265-274.
39. Sou YS, Waguri S, Iwata J, Ueno T, Fujimura T, et al. (2008) The Atg8 conjugation system is indispensable for proper development of autophagic isolation membranes in mice. Mol Biol Cell 19: 4762-4775.
40. Tanida I, Ueno T, Kominami E (2004) LC3 conjugation system in mammalian autophagy. Int J Biochem Cell Biol 36: 2503-2518.
41. Saitoh T, Fujita N, Jang MH, Uematsu S, Yang BG, et al. (2008) Loss of the autophagy protein Atg16L1 enhances endotoxin-induced IL-1beta production. Nature 456: 264-268.
42. Roy S, Maheshwari N, Chauhan R, Sen NK, Sharma A (2011) Structure prediction and functional characterization of secondary metabolite proteins of Ocimum. Bioinformation 6: 315-319.
43. Raazia R, Nijil RN (2017) Method for predicting transmembrane helices in protein sequences, international journal of engineering research & technology (ijert) ncetet 5.
44. Pyo JO, Jang MH, Kwon YK, Lee HJ, Jun JI, et al. (2005) Essential roles of Atg5 and FADD in autophagic cell death: dissection of autophagic cell death into vacuole formation and cell death. J Biol Chem 280: 20722-20729.
45. Nivetha R, Meenakumari M, Bhuvaragavan S, Hilda K, Janarthanan S (2021) In silico analysis of carbohydrate-binding pockets in the lectin genes from various species of Canavalia. Comput Biol Chem 92: 107477.
46. Komatsu M, Waguri S, Ueno T, Iwata J, Murata S, et al. (2005) Impairment of starvation-induced and constitutive autophagy in Atg7-deficient mice. J Cell Biol 169: 425-434.